

# Analysis of Coding Gain Due to In-Loop Reshaping

Chau-Wai Wong, *Member, IEEE*, Chang-Hong Fu, *Member, IEEE*, Mengting Xu,  
and Guan-Ming Su, *Senior Member, IEEE*

**Abstract**—Reshaping, a point operation that alters the characteristics of signals, has been shown capable of improving the compression ratio in video coding practices. Out-of-loop reshaping that directly modifies the input video signal was first adopted as the supplemental enhancement information (SEI) for the HEVC/H.265 without the need of altering the core design of the video codec. VVC/H.266 further improves the coding efficiency by adopting in-loop reshaping that modifies the residual signal being processed in the hybrid coding loop. In this paper, we theoretically analyze the rate–distortion performance of the in-loop reshaping and use experiments to verify the theoretical result. We prove that the in-loop reshaping can improve coding efficiency when the entropy coder adopted in the coding pipeline is suboptimal, which is in line with the practical scenarios that video codecs operate in. We derive the PSNR gain in a closed form and show that the theoretically predicted gain is consistent with that measured from experiments using standard testing video sequences.

**Index Terms**—In-loop Reshaping, Out-of-loop Reshaping, Quantization, Video Compression, VVC/H.266

## I. INTRODUCTION

The Joint Video Experts Team (JVET) started in 2017 the standardization process of Versatile Video Coding (VVC)/H.266 [1], aiming at a 50% bitrate reduction over the High Efficiency Video Coding (HEVC)/H.265 [2] while maintaining the subjective quality. Among various newly introduced coding tools, the *in-loop reshaping* [3] can improve the coding gain for both high dynamic range (HDR) [4] and standard dynamic range (SDR) [5], [6] video contents.

The use of the reshaping technique was initially motivated by the need to efficiently compress HDR video content using pre-HDR-era video codecs. Those video codecs were specifically designed and optimized for SDR videos and hence they do not perform well on HDR video content because of the mismatched characteristics between HDR and SDR videos. SDR videos typically have a dynamic range of luminance from 0.1 nits to 100 nits [7]. It does not fully exploit the maximum range that the human visual system can simultaneously resolve, which is of four orders of magnitude [7]. HDR videos, loosely defined as videos with a dynamic range

greater than that of SDR videos and with an extended color space named the wide color gamut (WCG), can significantly improve viewing experiences. Due to the different sensitivity of human eyes at different luminance levels, HDR videos are usually represented in an alternate luminance domain, e.g., the Perceptual Quantization (PQ) domain, rather than the Gamma domain traditionally used by SDR videos. If one alters the signal characteristics of HDR video signal to mimic those of the SDR videos, video codecs such as H.264/AVC [8] and HEVC/H.265 optimized for SDR videos can operate efficiently on HDR video contents.

The first well-accepted technique to improve the coding efficiency of HDR videos was the *out-of-loop* reshaping. A Call for Evidence (CfE) [9] was issued in February 2015 to evaluate the compression performance of the HEVC/H.265 on HDR/WCG videos and determine whether other promising technologies should be considered for future extensions of the standard. The call was partly to address the wide emergence of HDR/WCG content after the HEVC/H.265 standard had been finalized. Several proposals sharing similar ideas of using out-of-loop reshapers were submitted as responses [10]–[17], including approaches using a single layer and dual layers. In one joint response from Arris, Dolby, and Inter Digital [10], an adaptive intensity mapping was proposed as the pre- and postprocessing steps that encapsulate the HEVC/H.265 codec as illustrated in Fig. 1(a). The characteristics of the input HDR video signal are first analyzed and then mapped to cope with the standard characteristics expected by the HEVC/H.265 Main 10 Profile encoder. At the HEVC/H.265 decoder output, the signal is inversely mapped to reconstruct the HDR signal for display. As the pair of pre- and postprocessing mappings completely stay out of the hybrid video coding loops, such a strategy is named out-of-loop reshaping. The change was proposed as an add-on to HEVC/H.265 because any major modification to then dominating standard could be costly.

As the standardization process for VVC/H.266 began, it became feasible to make major codec changes such as moving the reshaping operation into the predictive coding loop. As time went on, several flaws in out-of-loop reshaping became evident to the video coding community. First, the out-of-loop reshaping approach significantly constrained the design and optimization of the reshapers. The design and optimization could not be jointly performed, leading to marginal performance gain. Second, the out-of-loop design led to the conformance point issue and end-to-end delay due to the extra postprocessing step. Third, it also had to introduce additional on-chip buffers in the decoder, which is costly. Because of the drawbacks and the opportunity from standardization, it was desirable to move the reshapers into the predictive coding loop for better coding gain and fewer issues. Fig. 1(b)

This work was supported in part by the China Scholarship Council (201806845028). (*Corresponding author: Chang-Hong Fu.*)

C.-W. Wong is with the Department of Electrical and Computer Engineering, NC State University, NC 27695 USA (e-mail: chauwai.wong@ncsu.edu).

C.-H. Fu is with the School of Electronic and Optical Engineering, Nanjing University of Science and Technology, Jiangsu 210094, China (e-mail: enchfu@njjust.edu.cn). He conducted the research work of this paper as a visiting scholar at the Dolby Laboratories.

M. Xu conducted this work when she was with the School of Electronic and Optical Engineering, Nanjing University of Science and Technology, Jiangsu 210094, China.

G.-M. Su is with Dolby Laboratories, Sunnyvale, CA 94085 USA (e-mail: guanmingsu@ieee.org).

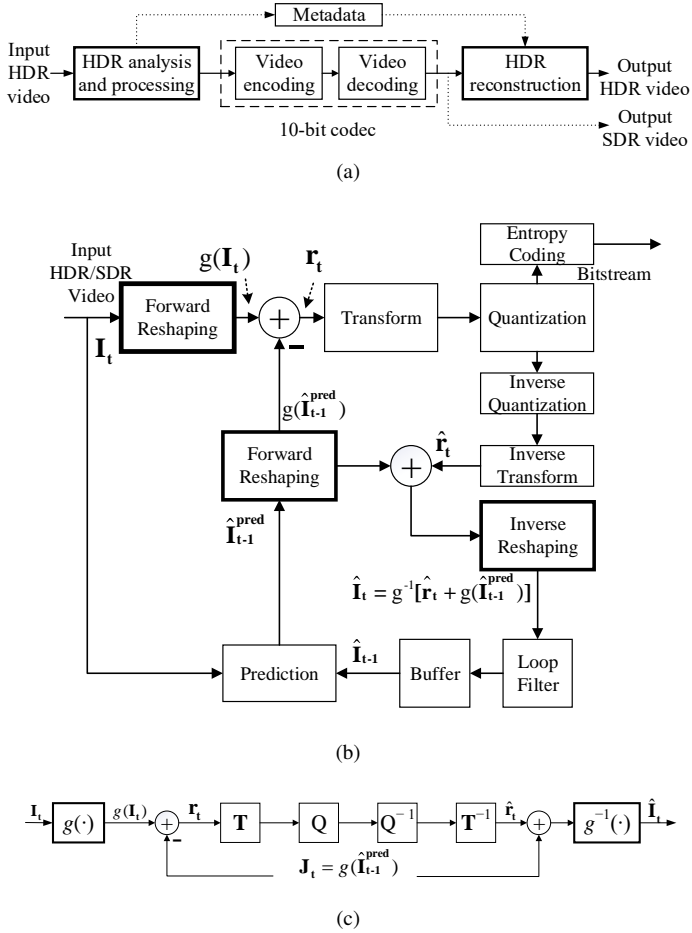


Fig. 1. Pipelines for video encoders with (a) out-of-loop reshapers and (b) in-loop reshapers. (c) Simplified schematic for the in-loop reshapers with blocks and symbols that are needed for the rate–distortion analysis.

illustrates an encoder with in-loop reshaping [4] proposed by Dolby for VVC/H.266. The forward and inverse mappings are incorporated into the encoder design. In-loop reshaping was shown to be effective for not only HDR videos [4], [18] but also SDR videos [5], [19]. The in-loop reshaping tool was further optimized and renamed as *luma mapping with chroma scaling (LMCS)* [20]–[22].

Although the in-loop reshapers had been known in video coding practices to improve the coding efficiency of HDR and SDR content [4], [5], [18], [19] and was later adopted by VVC/H.266 version 1 [23] in July 2020, no theoretical justification has been provided by the video coding community. Commonly asked questions include: (i) Why can SDR video contents benefit from in-loop reshaping, while there is no such issue as a characteristic mismatch between the expected input and real input? Recall that the characteristic mismatch between the HDR contents and pre-HDR-era codecs was the initial motivation for adopting reshapers. (ii) Where does the coding gain come from and which factors do the gain depend on? To address these questions, we will theoretically analyze a codec pipeline with an in-loop reshapers under a simplified reshaping scenario. We will express in an analytic form the distortion and bitrate and investigate the rate–distortion change before and after reshaping. We will also use test video sequences to

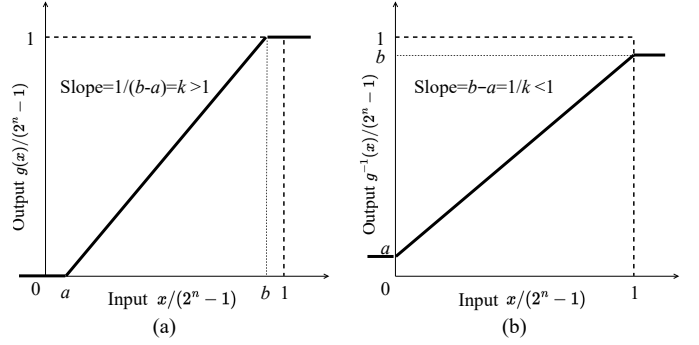


Fig. 2. A typical one-piece (a) forward reshaping function  $g(x) \in [0, 2^n - 1]$  and (b) its corresponding inverse reshaping function  $g^{-1}(x) \in (2^n - 1) \cdot [a, b]$ , where  $0 < a < b < 1$ .

validate our theoretical model and result. The key contribution of the paper is that, for the first time, the coding gain brought by the in-loop reshaping is theoretically justified. Our analysis shows that such gain is independent of characteristics of the data (HDR or SDR, PQ or Gamma domain) and is a byproduct of the use of suboptimal entropy coders. We note that theoretical result holds even for the simplified reshaping scenario of using a one-piece reshaping function, i.e., a bounded range-expansion operation, instead of using a well-tuned multi-piece function adopted in VVC/H.266 [23]. The analysis is amendable to multi-piece functions, which we leave for future work.

The rest of the paper is organized as follows. In Section II, we present the theoretical analysis. In Section III, we use testing video sequences to verify the theoretical result. In Section IV, we discuss some common concerns. In Section V, we conclude the paper.

## II. CODEC WITH IN-LOOP RESHAPER

Fig. 1(b) illustrates how in-loop reshaping blocks, i.e., those highlighted with thicker borders, may be incorporated into a standard hybrid video coding encoder. We follow the decoder definition in [6, Fig. 4] and extrapolated a complete encoder schematic accordingly. Here, the forward reshaping function (or the forward reshapers) is a monotonically nondecreasing function  $g(x)$  that acts elementwise on a raw or predicted input video signal to maximize its range. Reshaping is more commonly known as point processing in the image processing literature [24, Ch. 3.1.1]. Fig. 2 shows an example of the forward reshaping function  $g$ , in which the range  $(2^n - 1) \cdot [a, b]$  of an input signal will be linearly mapped to the range of  $(2^n - 1) \cdot [0, 1]$ . For example, to expand the range of 8-bit video input to the maximum possible range, the output of  $g(x)$  should range from 0 to 255. Conversely, the inverse reshaping function (or the inverse reshapers)  $g^{-1}(x)$  compresses the full-range reconstructed video signal back to the range of the raw video signal.

As illustrated in Fig. 1(b), the forward reshapers maps the raw frame  $\mathbf{I}_t$  and predicted frame  $\hat{\mathbf{I}}_{t-1}^{\text{pred}}$  into a reshaped domain before the residual frame  $\mathbf{r}_t$  is calculated. The transform coding, quantization, and frame reconstruction all operate in the reshaped domain. The inverse reshapers maps the

reconstructed frame back to the nonreshaped domain for deblocking, buffering, display, and motion compensation. In practical schemes,  $g$  is a nonlinear, oftentimes implemented by a multipiece linear function [1], [25]. We will see from both the theoretical analysis and experiments of this paper that even if the nonlinear mapping has only one piece as in Fig. 2, there will be a gain in coding efficiency.

We simplify Fig. 1(b) by removing processes/blocks that are irrelevant to the rate–distortion analysis. An equivalent diagram with symbols similarly defined as in [26] is shown in Fig. 1(c).  $\mathbf{I}_t$  and  $\hat{\mathbf{I}}_t \in [0, 2^n - 1]$  are the raw frame to be encoded and the reconstructed frame at time  $t$  in the nonreshaped domain.  $g(\cdot)$  is the deterministic forward reshaping function.  $\hat{\mathbf{I}}_{t-1}^{\text{pred}}$  is the motion compensated frame in the nonreshaped domain. The raw residual frame  $\mathbf{r}_t$  is generated by subtracting the reshaped motion-compensated frame  $\mathbf{J}_t \stackrel{\text{def}}{=} g(\hat{\mathbf{I}}_{t-1}^{\text{pred}})$  from the reshaped raw frame  $g(\mathbf{I}_t)$ .  $\mathbf{T}$  is the forward transform.  $\mathcal{Q}(\cdot)$  and  $\mathcal{Q}^{-1}(\cdot)$  are the elementwise quantization and the dequantization operations. We will use their composition, namely, the quantizer  $\mathcal{Q}(\cdot) = \mathcal{Q}^{-1}[\mathcal{Q}(\cdot)]$ , for the following analysis.  $\hat{\mathbf{r}}_t$  is the reconstructed residual frame in the reshaped domain.

To simplify the mathematical notations resulting from the left and right matrix multiplications of 2-d transforms, we vectorize frames and create a combined transform matrix. Specifically, all  $N$ -by- $N$  image pixels are vectorized into a column vector of length  $N^2$  by stacking from the first to the last columns, and the corresponding horizontal transform  $\mathbf{H}$  and vertical transform  $\mathbf{H}^T$  of size  $N$ -by- $N$  can be represented by the  $N^2$ -by- $N^2$  transform matrix  $\mathbf{T} = \mathbf{H} \otimes \mathbf{H}^T$  [27], where  $\otimes$  is the Kronecker product.

#### A. Distortion Reduction Due to Range Expansion

We write the relations among symbols of the equivalent diagram in Fig. 1(c) from left to right as follows:

$$\mathbf{r}_t = g(\mathbf{I}_t) - g(\hat{\mathbf{I}}_{t-1}^{\text{pred}}), \quad (1a)$$

$$\hat{\mathbf{r}}_t = \mathbf{T}^{-1} \mathcal{Q}(\mathbf{Tr}_t), \quad (1b)$$

$$\hat{\mathbf{I}}_t = g^{-1}(\hat{\mathbf{r}}_t + g(\hat{\mathbf{I}}_{t-1}^{\text{pred}})). \quad (1c)$$

Substituting the reconstructed residual frame (1b) into (1c), we obtain:

$$\hat{\mathbf{I}}_t = g^{-1} \left[ \mathbf{T}^{-1} \mathcal{Q}(\mathbf{Tr}_t) + g(\hat{\mathbf{I}}_{t-1}^{\text{pred}}) \right] \quad (2a)$$

$$= g^{-1} \left[ \mathbf{T}^{-1} [\mathbf{Tr}_t + q \cdot e(\mathbf{Tr}_t/q)] + g(\hat{\mathbf{I}}_{t-1}^{\text{pred}}) \right] \quad (2b)$$

$$= g^{-1} [g(\mathbf{I}_t) + \mathbf{T}^{-1} q \cdot e(\mathbf{Tr}_t/q)], \quad (2c)$$

where (2c) can be obtained using (1a), and (2b) can be obtained by using the definition of the quantizer that decomposes the quantized result  $\mathcal{Q}(x)$  into the sum of the raw input  $x$  and a rounding residue as follows:

$$\mathcal{Q}(x) = q \cdot \text{round}(x/q) = x + q \cdot e(x/q), \quad (3)$$

where  $q \in \mathbb{R}^+$  is the quantization step,  $\text{round}(\cdot)$  is the rounding to the nearest integer operation, and the rounding residue  $e(x)$  is defined as follows:

$$e(x) = \text{round}(x) - x, \quad e(x) \in (-1/2, 1/2]. \quad (4)$$

We focus on the simplest case that there is only one nonflat linear segment in the reshaping function as shown in Fig. 2, namely,

$$g(x) = \begin{cases} 0, & x \in (2^n - 1) \cdot [0, a), \\ kx, & x \in (2^n - 1) \cdot [a, b], \\ 1, & x \in (2^n - 1) \cdot (b, 1], \end{cases} \quad (5)$$

where  $0 < a < b < 1$  and  $k = 1/(b - a) > 1$  for range expansion. We further simplify (2c) as follows:

$$\hat{\mathbf{I}}_t = g^{-1} [k \cdot \mathbf{I}_t + \mathbf{T}^{-1} q \cdot e(\mathbf{Tr}_t/q)] \quad (6a)$$

$$\approx \mathbf{I}_t - k^{-1} \mathbf{T}^{-1} q \cdot e(\mathbf{Tr}_t/q), \quad (6b)$$

where the approximation is caused by the coordinates of the input to  $g^{-1}$  in (6a) whose values are less than 0 or greater than  $2^n - 1$ .<sup>1</sup> These cases are of low likelihood and practically do not result in large reconstruction errors, so we ignore this detail in this first effort in studying the in-loop reshaping.

Hence, the reconstructed squared error for frame  $\mathbf{I}_t$  can be calculated as follows using (6b):

$$\|\hat{\mathbf{I}}_t - \mathbf{I}_t\|^2 \approx \left\| k^{-1} \mathbf{T}^{-1} q \cdot e(\mathbf{Tr}_t/q) \right\|^2 \quad (7a)$$

$$= (q/k)^2 \left\| e(\mathbf{Tr}_t/q) \right\|^2. \quad (7b)$$

Note that  $\mathbf{T}^{-1}$  disappears from the expression as it is an orthogonal matrix that does not affect the norm of any vector it multiplies to. The rounding residue function  $e(\cdot)$  is applied elementwise to each pixel of the  $(1/q)$ -scaled transformed residual frame  $\mathbf{Tr}_t/q$ , resulting  $N^2$  nearly uncorrelated random variables uniformly distributed from  $-1/2$  to  $1/2$ . We define  $\text{MSE}(\hat{\mathbf{I}}_t, \mathbf{I}_t)$  as the expected mean squared error averaged over all pixel locations in a frame, namely,

$$\text{MSE}(\hat{\mathbf{I}}_t, \mathbf{I}_t) = \mathbb{E} \left[ \frac{1}{N^2} \|\hat{\mathbf{I}}_t - \mathbf{I}_t\|^2 \right] = k^{-2} \cdot \frac{q^2}{12}. \quad (8)$$

The above result reveals that when there is no reshaping, i.e.,  $k = 1$ , the MSE expression degenerates to  $q^2/12$ , a well-known result for a uniform quantizer being used in high-rate scenarios [28]. Our result in (8) shows that the in-loop resaper is effective in reducing the MSE by a multiplicative factor of  $k^{-2} < 1$  in the range expansion scenarios.

#### B. Entropy Increase Due to Range Expansion

We first mathematically analyze the entropy before and after reshaping, then extend the results to the bitrate by assuming the practical entropy coder used in video coding has a rate that is consistently higher than the entropy through a nonlinear, deterministic mapping.

We exploit the differential entropy to enable analytic tractability for analyzing the entropy of quantized random variables. Except for the cases of uniform random variables, it is in general difficult to obtain an analytic expression of the entropy of a quantized random variable. Let us denote a quantized

<sup>1</sup>If both  $g(x)$  and  $g^{-1}(x)$  are linear and inverse functions of each other over  $\mathbb{R}$ , the approximation in (6b) will become equality. However, as the example in Fig. 2 reveals, neither  $g(x)$  nor  $g^{-1}(x)$  has an inverse function due to the clipping branches in their definitions.

random variable  $X^q$  obtained from quantizing a continuous random variable  $X$  with step  $q$ . The differential entropy of the random variable  $X$  is defined using its probability density function (PDF)  $f_X(x)$  [29, Ch. 8] as follows:

$$h(X) = - \int_{-\infty}^{\infty} f_X(x) \log_2 f_X(x) dx, \quad (9)$$

which is a fixed number for a given PDF with fixed parameters. The discrete entropy of the corresponding quantized random variable  $X^q$  can be approximated by the differential entropy of  $X$  and an offset quantity related to the quantization step [29, Thm. 8.3.1], namely,

$$H(X^q) \approx h(X) - \log_2 q, \quad (10)$$

where  $H(X^q)$  is the discrete entropy of  $X$  after being quantized with step  $q$ . The theorem reveals that the entropy is determined by (i) the shape of the PDF of  $X$ , i.e., the fixed number  $h(X)$  when  $X$  is given, and (ii) and the accuracy of the quantization, i.e., the number of bits needed to represent the uniformly spaced levels in a unit interval. The approximation in (10) becomes more accurate as the quantizer becomes finer and it becomes exact as  $q \rightarrow 0$  [29, Thm. 8.3.1]. This theoretical insight is consistent with the observation that more quantized levels lead to larger discrete entropy  $H(X^q)$ .

1) *No Gain Using Optimal Entropy Coder*: The PDFs for residual frames before and after reshaping are denoted by  $f_X(x)$  and  $f_Y(y)$ , respectively. Given the reshaping function  $g(X) = kX = Y$  and applying the formula for random variable transformation [30, Ch. 4.7], the two PDFs are related as follows:

$$f_Y(y) = k^{-1} f_X(y/k). \quad (11)$$

The differential entropies before and after reshaping are

$$h^{(0)} = - \int_{\mathbb{R}} f(x) \log_2 f(x) dx, \quad (12a)$$

$$h^{(1)} = - \int_{\mathbb{R}} k^{-1} f(y/k) \log_2 [k^{-1} f(y/k)] dy \quad (12b)$$

$$= - \int_{\mathbb{R}} f(\xi) \log_2 \left[ \frac{1}{k} f(\xi) \right] d\xi, \quad (12c)$$

where  $f(x)$  denotes  $f_X(x)$  for simplicity and can have either a finite or infinity support, and (12c) is obtained by a change of variable,  $\xi \leftarrow y/k$ . The change of the differential entropy due to reshaping is therefore:

$$h^{(1)} - h^{(0)} = - \int_{\mathbb{R}} f(x) \log_2 \left( \frac{1}{k} \right) dx = \log_2 k > 0, \quad (13)$$

where we assume  $k > 1$ , the range expansion scenario.

The theorem in (10) reveals that the difference between differential entropy converges to the difference between entropy as the quantizer becomes finer, namely,

$$h^{(1)} - h^{(0)} \approx H^{(1)} - H^{(0)}. \quad (14)$$

Together with (13), we obtain

$$H^{(1)} \approx H^{(0)} + \log_2 k. \quad (15)$$

Hence, we conclude that the range expansion due to reshaping increases the entropy by roughly  $\log_2 k$ .

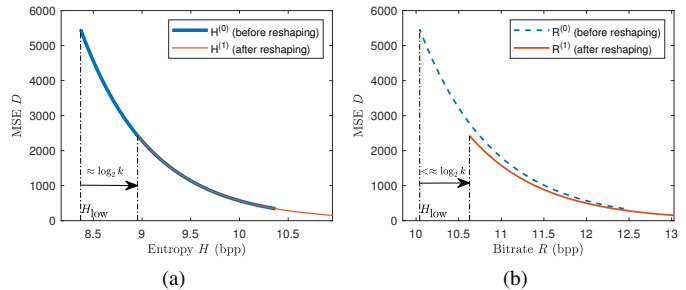


Fig. 3. (a) MSE–entropy (H–D) curves overlap before and after reshaping, indicating that reshaping does not lead to coding gain for optimal entropy coders. (b) MSE–bitrate (R–D) curves before and after reshaping with a range expansion factor  $k = 1.5$  for a suboptimal entropy coder with a slope ratio  $\eta = 0.83$ . The gap indicates that reshaping can lead to coding gain for a suboptimal entropy coder.

When assuming the uniform distribution for the residual frame,  $H^{(0)} = - \sum p_i \log_2 p_i = \log_2 M$ , and  $M = \text{round}(2^n/q)$  is the number of codewords for  $n$ -bit videos, we obtain

$$H^{(1)} \approx \log_2 \left( \frac{2^n}{q/k} \right). \quad (16)$$

For Gaussian distribution with variance  $\sigma^2$  (regardless the range of the support if the tails are not significantly cut off),  $h^{(0)} = \frac{1}{2} \log_2(2\pi e \sigma^2)$  [29, Ch. 8.1], where  $e$  is Euler's number. Combining with  $H^{(0)} \approx h^{(0)} - \log_2 q$  and (15), we have

$$H^{(1)} \approx \log_2 \left( \frac{\sqrt{2\pi e} \sigma}{q/k} \right). \quad (17)$$

We will show in Part 2) that even though the distribution type affects the shape of rate–distortion curves, the PSNR gain is independent of the distribution type.

Recall in the MSE derivation in (8), we have shown that  $\text{MSE} = (q/k)^2/12$ , hence the (entropy, distortion) points before and after reshaping when assuming the uniform distribution can be written as follows:

$$(H^{(0)}, D^{(0)}) = \left( \log_2 \left( \frac{2^n}{q} \right), \frac{q^2}{12} \right), \quad (18a)$$

$$(H^{(1)}, D^{(1)}) = \left( \log_2 \left( \frac{2^n}{q/k} \right), \frac{(q/k)^2}{12} \right). \quad (18b)$$

It is easy to show that for both cases, the H–D curves have the following expression:

$$D = \frac{1}{12} \cdot 2^{-2(H-n)}, \quad (19)$$

except that they have shifted supports  $\mathcal{H}^{(0)} = [H_{\text{low}}, H_{\text{high}}]$  and  $\mathcal{H}^{(1)} = \mathcal{H}^{(0)} + \log_2 k$ , respectively. Here,  $H_{\text{low}}$  and  $H_{\text{high}}$  are the lower and upper limits for the interval  $\mathcal{H}^{(0)}$ , respectively. Fig. 3(a) illustrates a pair of H–D curves before reshaping (blue) and after reshaping (red). Hence, we conclude that if optimal entropy coder is used, i.e., rate equals entropy, reshaping will not bring gain in the rate–distortion sense given that the operating point merely moves along the same H–D curve.

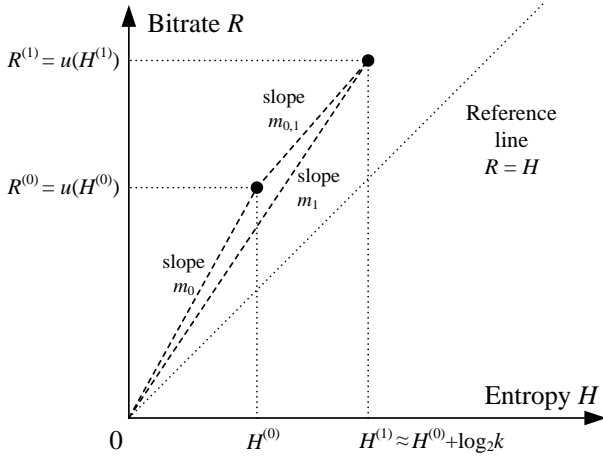


Fig. 4. Operating points  $(H^{(0)}, R^{(0)})$  and  $(H^{(1)}, R^{(1)})$  on bitrate function  $u(\cdot)$  (not shown for clarity) before and after reshaping on the bitrate–entropy plane, respectively. The secant from the origin to  $(H^{(0)}, R^{(0)})$  has a slope of  $m_0 > 1$  and the secant from  $(H^{(0)}, R^{(0)})$  to  $(H^{(1)}, R^{(1)})$  has a slope of  $1 \leq m_{0,1} < m_1$ . The very fact that the slope ratio  $\eta = m_{0,1}/m_0 < 1$  ensures that reshaping can always lead to coding gain when suboptimal entropy coders are used.

2) *Gain Due to Suboptimal Entropy Coder:* Entropy coders are almost always suboptimal especially in real applications. Mathematically, we define a *bitrate function*  $u(\cdot)$  of a practical entropy coder relating the bitrate  $R$  and the entropy  $H$ , which must satisfy the following relation:

$$R = u(H) > H. \quad (20)$$

In the bitrate–entropy (R–H) plane of Fig. 4, all possible  $u(\cdot)$  (not shown to reduce the complexity of the figure) will result in operating points laying in the upper half region above the line of  $R = H$ . For a given video codec with bitrate function  $u(\cdot)$ , we use points  $(H^{(0)}, R^{(0)})$  and  $(H^{(1)}, R^{(1)})$  to denote the operating conditions before and after reshaping, respectively:

$$R^{(0)} = u(H^{(0)}), \quad (21a)$$

$$R^{(1)} = u(H^{(1)}). \quad (21b)$$

Using (21a) and (20), it is immediate that the slope  $m_0$  of the secant line for  $u(\cdot)$  between  $(0, 0)$  and  $(H^{(0)}, R^{(0)})$  satisfy the following relation:

$$m_0 \stackrel{\text{def}}{=} R^{(0)}/H^{(0)} \in (1, \infty). \quad (22)$$

Similarly, we define the slope  $m_1$  of the secant line for  $u(\cdot)$  between  $(0, 0)$  and  $(H^{(1)}, R^{(1)})$  as

$$m_1 \stackrel{\text{def}}{=} R^{(1)}/H^{(1)} \in (1, m_0). \quad (23)$$

Here, we assume that  $m_1$  is upper bounded by  $m_0$  because the entropy coder is likely to be more efficient when operating at  $(H^{(1)}, R^{(1)})$  after reshaping than at  $(H^{(0)}, R^{(0)})$  before reshaping. We explain in more detail using HDR video compression as an example. When encoding reshaped signals, the residual values are modified by the resaper to be distributed across the full range of the domain, which resembles the statistics of SDR videos that a video codec is optimized on. In contrast, when encoding nonreshaped HDR signals that have

different statistics from those of SDR signals, the entropy coder is likely to work less efficiently for the residual values not distributing across the full range of the domain. We also define the slope  $m_{0,1}$  of the secant line for  $u(\cdot)$  between  $(H^{(0)}, R^{(0)})$  and  $(H^{(1)}, R^{(1)})$  as

$$m_{0,1} \stackrel{\text{def}}{=} \frac{R^{(1)} - R^{(0)}}{H^{(1)} - H^{(0)}} \in [1, m_1]. \quad (24)$$

Here, the upper bound of  $m_{0,1} < m_1$  is due to the geometry of the triangle formed by the origin and the two operating points. The lower bound of  $m_{0,1} \geq 1$  is reasonable since the increase in bitrate should be at least comparable to the increase in entropy.

Given the definitions of the slopes of the three secant lines, we can continue to simplify the relation after reshaping described in (21b) as follows:

$$R^{(1)} = u(H^{(1)}) \quad (25a)$$

$$\approx u(H^{(0)} + \log_2 k) \quad (25b)$$

$$\approx u(H^{(0)}) + m_{0,1} \cdot \log_2 k \quad (25c)$$

$$= m_0 \cdot H^{(0)} + (\eta \cdot m_0) \log_2 k \quad (25d)$$

$$\approx m_0 \cdot (h^{(0)} - \log_2 q) + (\eta \cdot m_0) \log_2 k \quad (25e)$$

$$= \log_2 \left( \frac{2^{n+h^{(0)}}}{q/k^\eta} \right)^{m_0}, \quad (25f)$$

where (25b) is due to the information-theoretic approximation (15), (25c) is due to the geometry, and (25e) is due to the approximation of discrete entropy by differential entropy in (10). In (25d), we introduce the *slope ratio*  $\eta$  defined as

$$\eta = m_{0,1}/m_0 \in (0, 1), \quad (26)$$

where the upper bound is due to  $m_{0,1} < m_1 < m_0$ . The slope ratio  $\eta$  may partially reflect the optimality of the entropy coder. For example, for an optimal entropy coder, all operating points should be on  $R = H$ , hence  $\eta = 1$ . As we will see later, the slope ratio  $\eta$  is one of the only two factors that determine the PSNR gain. Reorganizing (25f), we obtain the rate–distortion operating points before and after reshaping for a nonideal entropy coder as follows:

$$(R^{(0)}, D^{(0)}) = \left( \log_2 \left( \frac{2^{n+h^{(0)}}}{q} \right)^{m_0}, \frac{q^2}{12} \right), \quad (27a)$$

$$(R^{(1)}, D^{(1)}) = \left( \log_2 \left( \frac{2^{n+h^{(0)}}}{q/k^\eta} \right)^{m_0}, \frac{(q/k)^2}{12} \right). \quad (27b)$$

It is easy to show via canceling the quantizer step  $q$  that the R–D curves have different expressions before and after expansions as follows:

$$D = \frac{1}{12} \cdot 2^{-2[R/m_0 - (n+h^{(0)})]}, \quad (28a)$$

$$D = \frac{1}{12} \cdot 2^{-2[R/m_0 - (n+h^{(0)})]} \cdot k^{2(\eta-1)}. \quad (28b)$$

Hence, the gain in PSNR given the same bitrate  $R$  is

$$\Delta \text{PSNR} = 10 \log_{10} (D^{(0)}/D^{(1)}) = 20(1 - \eta) \log_{10} k. \quad (29)$$

TABLE I  
THEORETICALLY CALCULATED PSNR GAIN

$\eta$	$k$	$\Delta\text{PSNR}$ (dB)
0.95	2.0	0.30
0.98	2.0	0.12
0.95	1.8	0.26
0.98	1.8	0.10
1	Any value	0

Note that the PSNR gain is dependent on the slope ratio  $\eta$  and the reshaping scalar  $k$ , but independent of its differential entropy  $h^{(0)}$ , i.e., the shape of the histogram of the residual signal before reshaping. The PSNR gain is also independent of the bitrate  $R$  specific to the current operating condition hence theoretically, the gain is uniform over  $R$ . TABLE I illustrates a few calculated examples of the PSNR gain under typical values for  $\eta$  and  $k$ . Fig. 3(b) illustrates a pair of simulated R–D curves with range expansion factor  $k = 1.5$  when the suboptimality of the entropy coder is configured to have  $m_0 = 1.2$  and  $m_{0,1} = 1$ . The R–D curve after reshaping has a better rate–distortion trade-off as predicted by our theory.

### III. EXPERIMENTAL RESULTS ON TEST SEQUENCES

#### A. Use of Simplified Video Codec

To verify the theoretical PSNR gain due to in-loop reshaping as predicted by our theoretical result in (29), we implemented a simplified video codec with an IPP... group-of-pictures structure with the macroblock size of  $16 \times 16$  and the DCT size of  $8 \times 8$ . Since any practical video codec is suboptimal, our simplified codec can allow us to calculate the two entropy–bitrate points before and after reshaping as illustrated in Fig. 4. An off-the-shelf codec such as VVC/H.266 was not used because its sophisticated structure makes it difficult to calculate the corresponding entropy and bitrate. The entropy coder in our implementation is customized to allow tuning the degree of suboptimality of the coder, which allows us to comprehensively verify the theoretical result (29) from the previous section.

The block diagram of the codec is shown in Fig. 1(b). Motion estimation with full search and motion compensation are performed for each macroblock in P frames. A search range is determined per test sequence based on the statistics of motion vectors extracted from HEVC/H.265 compressed files. Residual blocks are DCT-transformed and quantized. Arithmetic coding is then performed on the quantized DCT coefficients to obtain the bitrate. Meanwhile, entropy is calculated based on the histogram of codewords/quantized coefficients. In order to approximate the adaptive behavior of context-based adaptive binary arithmetic coding (CABAC) used in standardized video codecs, we construct the histogram of codewords at the frame level. The three reshaping blocks with thick border in Fig. 1(b) are bypassed if reshaping is turned off.

#### B. Experimental Conditions

Using the simplified video codec, we were able to verify the proposed theoretical model on standard test sequences BAS-

KETBALLDRILL, BQMALL, FOURPEOPLE, KRISTENAND-SARA, PARTYSCENE, and VIDYO. For the choices of QPs and quantizer steps  $q$ , we adopted those specified in the H.264/AVC standard.

To experimentally measure the PSNR gain, we first connect a set of experimentally obtained R–D points under different QPs using a piecewise linear line for estimating R–D curves before and after reshaping. We then use the bitrate that corresponds to the middle of the tested QP range to find the PSNR gain and consider it as the real/measured PSNR gain. To obtain the theoretically predicted gain, we need the slope ratio  $\eta$  and the reshaping range expansion factor  $k$  in (29). To estimate  $\eta$ , we use the estimates for slopes  $m_0$  and  $m_{0,1}$ . The expansion factor  $k$  is estimated from the supports of the histograms before and after the range expansion.

#### C. Rate–Distortion Performance and Predicted Gain

We use the BASKETBALLDRILL sequence as an example in Fig. 5 to describe the experimental results and explain the connection to the theoretical result. Fig. 5(a) reveals that reshaping leads to increases in both PSNR and bitrate, and more importantly, the R–D points after range expansion (in red “x”) sit to the top-right of the original R–D points (in blue “o”). We annotated the shift of one such operating point. Specifically, the right arrow in Fig. 5(a) shows that the increase of bitrate due to reshaping is 0.83 bits, which is less than the largest possible improvement of  $\log_2 1.95 = 0.96$  bits in terms of entropy, in which we plug the measured range expansion factor  $\hat{k} = 1.95$  into the theoretical results of (15). Fig. 5(b) zooms into the middle range of Fig. 5(a), which clearly shows that the new R–D curve has a higher PSNR than the original R–D curve at the same bitrate. The experimental results support a positive coding gain as predicted by our theoretical model. We note that Fig. 5(a)–(b) experimentally verify the theoretical results in (27)–(28) and the simulated results in Fig. 3(b).

Fig. 5(c) shows an R–H curve resulting from encoding the BASKETBALLDRILL sequence and its shape validates our statement in (20) about the suboptimality of entropy coders. The empirical R–H curve sits above the reference line of  $R = H$ , which experimentally verifies the theoretical illustration in Fig. 4. Such suboptimality revealed by the R–H curve will lead to the gain in coding efficiency as our theory in (29) predicts.

To calculate the slope ratio  $\eta$  from the empirically obtained R–H curve in Fig. 5(c), we pick two operating points on the curve. First, we use the measured bitrate before reshaping,  $\hat{R}^{(0)}$ , to find the estimated entropy before reshaping,  $\hat{H}^{(0)}$ . See the annotated blue circle positioned at  $(\hat{H}^{(0)}, \hat{R}^{(0)})$ . Second, the estimated entropy after reshaping calculated as  $\hat{H}^{(1)} = \hat{H}^{(0)} + \log_2 \hat{k}$ , where  $\hat{k}$  is the estimated reshaping range expansion factor. Third, the estimated bitrate after reshaping  $\hat{R}^{(1)}$  can then be read from the curve. See the annotated red dot positioned at  $(\hat{H}^{(1)}, \hat{R}^{(1)})$  in Fig. 5(c). Finally, an estimate for  $\eta$  may be calculated per (26), (24), and (22) as follows:

$$\hat{\eta} = \frac{\hat{R}^{(1)} - \hat{R}^{(0)}}{\hat{H}^{(1)} - \hat{H}^{(0)}} \bigg/ \frac{\hat{R}^{(0)}}{\hat{H}^{(0)}} = \left( \frac{\hat{R}^{(1)}}{\hat{R}^{(0)}} - 1 \right) \frac{\hat{H}^{(0)}}{\log_2 \hat{k}}. \quad (30)$$

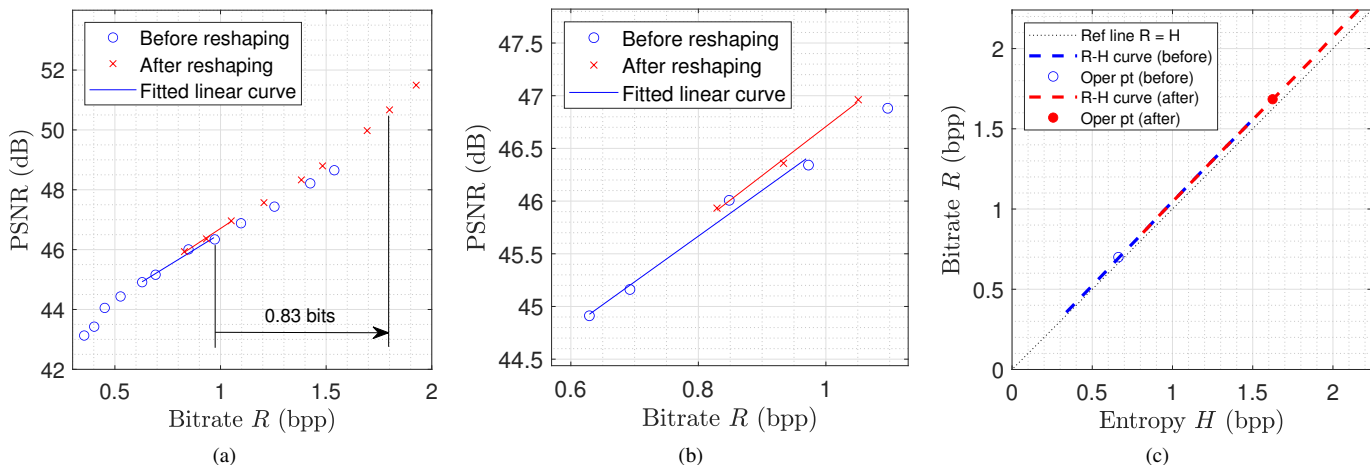


Fig. 5. Example plots from sequence BASKETBALLDRILL for measuring (a)–(b) the empirical PSNR gain and (c) the quantities needed for predicting the theoretical PSNR gain. (a) Rate–distortion (R–D) curves before and after reshaping. Each circle corresponds to a specific quantization step. (b) Zoomed-in version of (a). The plots reveal that reshaping causes the R–D curve to move to the top-right corner of the R–D plane, leading to an increased measured/empirical PSNR as predicted by our theoretical result (29). (c) Corresponding bitrate–entropy (R–H) curve, which is contributed by the R–H points before (blue dashed) and after (red dashed) reshaping. The R–H curve sits above the diagonal line, confirming the suboptimality of the entropy coder stated in (20). The two operating points  $(\hat{H}^{(0)}, \hat{R}^{(0)})$  (“o”) and  $(\hat{H}^{(1)}, \hat{R}^{(1)})$  (“•”) for predicting the theoretical PSNR gain are annotated on the R–H curve.

Plugging  $\hat{\eta}$  into (29), we obtain the predicted PSNR gain for one frame. The process is repeated for a total of 19 P frames of each subsequence, which results in 19 pairs of theoretically predicted gain and measured gain. Each video sequence contains 300–400 frames or 15–20 subsequences. In Fig. 6, for each of the six testing video sequences, we show two typical scatter plots between predicted gain and measured gain for one subsequence each. More scatter plots can be generated by running our plotting source code.<sup>2</sup> Each circle in a scatter plot corresponds to the PSNR gain of a frame in the middle of the tested QP range. Since all circles fall within the first quad of the 2-D plane, we conclude that for all frames, PSNR gains from the theory and actual measurement are consistently positive. To provide a comprehensive evaluation of all subsequences, TABLE II further provides quantitative results on the measured PSNR gain and predicted PSNR gain. Each cell of measured/predicted gain contains the average and standard deviation of the increased PSNR values from all subsequences of a test sequence. Even though the predicted PSNR gain may overestimate or underestimate the measured gain, our theoretical model is capable of correctly predicting the sign of the gain for almost all subsequences that were tested.

We also calculate the cosine similarity [31] for each subsequence and plot them against the starting index of the corresponding subsequence in Fig. 6. The average and standard deviation of the cosine similarity values of each sequence are given in the right-most column of TABLE II. We note that for 5 of 6 testing sequences, the cosine similarities of all subsequences are close to 1. Even though a small proportion of subsequences in BASKETBALLDRILL have smaller

<sup>2</sup>Source code for the main program and for plotting are available at <https://ncsu-cwwong.org/projects/reshaping/> for paper review purposes. Once the paper is accepted, the source code will be released on GitHub.

TABLE II  
MEASURED AND THEORETICALLY PREDICTED PSNR GAINS.

Sequence	Slope $k$	Rate (bit)	PSNR Gain in dB		Cosine Similarity
			Measured	Predicted	
BasketballDrill	1.95	0.7	0.10 (0.06) <sup>†</sup>	0.26 (0.03)	0.70 (0.43)
BQMall	1.95	1.4	0.25 (0.06)	0.18 (0.03)	0.99 (0.01)
FourPeople	1.93	0.8	0.30 (0.02)	0.07 (0.01)	0.99 (0.01)
Kristen&Sara	1.93	0.9	0.40 (0.04)	0.06 (0.01)	0.99 (0.01)
PartyScene	1.95	1.9	0.15 (0.02)	0.19 (0.01)	0.98 (0.05)
Vidyo	1.98	0.7	0.38 (0.06)	0.12 (0.01)	0.90 (0.03)

<sup>†</sup> Each reported PSNR gain is averaged over all subsequences and the sample standard deviation is reported within the following parentheses.

cosine similarity, the majority of subsequences in this testing sequence perform as expected. We therefore confirm that our theoretical model about the PSNR gain is consistent with the experimental results.

#### D. Impact of Suboptimal Entropy Coder on Coding Gain

In this subsection, we experimentally verify that a less optimal entropy coder can lead to a larger coding gain due to reshaping. We control the degree of suboptimality of the entropy coder by changing the granularity of the codewords of arithmetic coding. Specifically, in the baseline suboptimal entropy coder that is also used in other sections of this paper, the codewords were quantized with a step size of 100, whereas in “More Optimal” and “Less Optimal” setups in TABLE III, they have quantizing step sizes of 10 and 1000, respectively. TABLE III shows the measured PSNR gains for each sequence at different suboptimality levels. The table reveals an increasing trend in coding gain as the entropy coder becomes less optimal, which confirms that reshaping can achieve more gain for entropy coders that are less optimal.

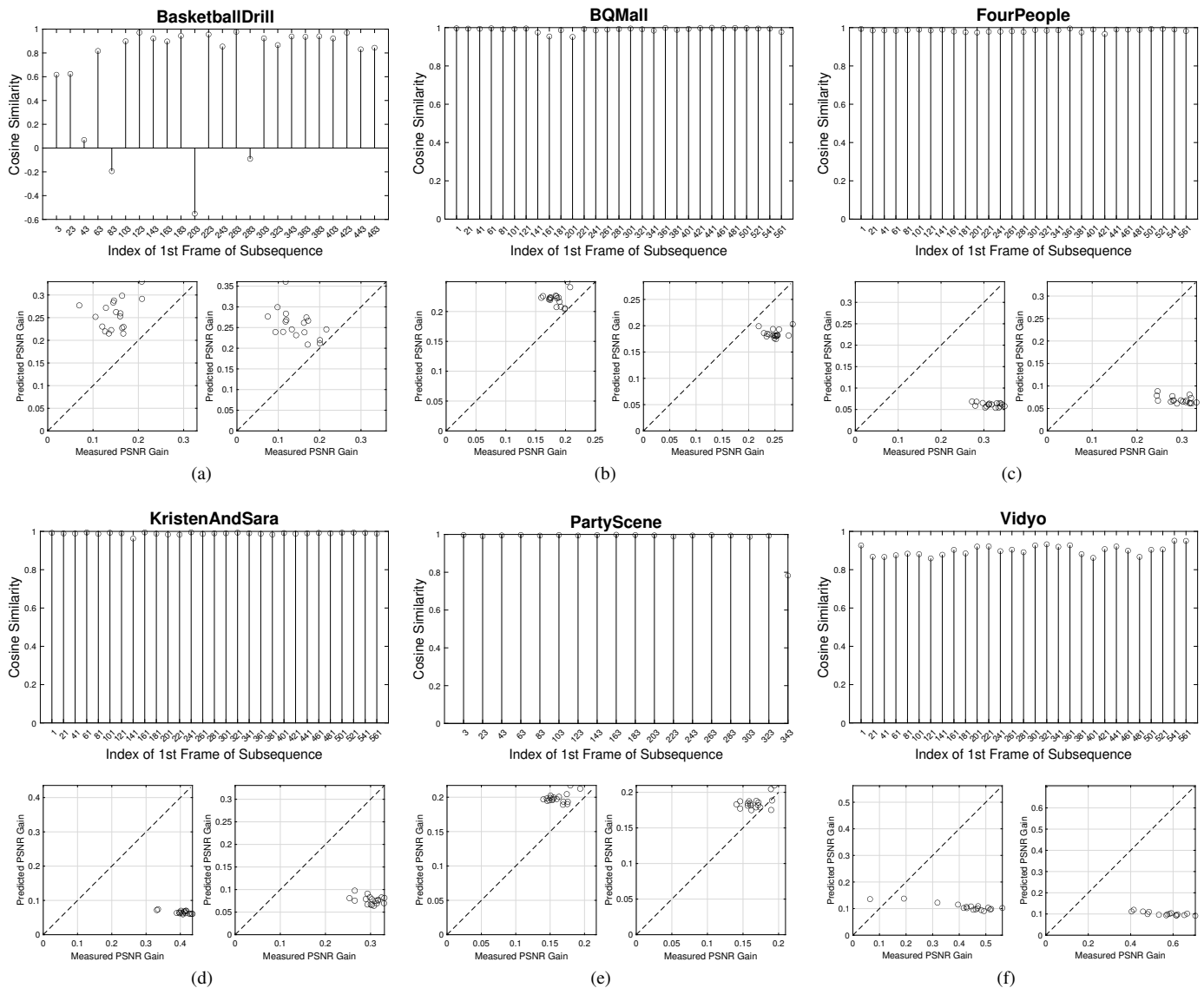


Fig. 6. Each subfigure from (a) to (f) contain a top plot of cosine similarity values for all test videos' subsequences and two bottom plots of typical scatter plots between measured gain and theoretically predicted gain. Each circle corresponds to the PSNR gain of a frame at a certain bitrate. PSNR gains from the theory and actual measurement are consistently positive in terms of cosine similarity.

TABLE III  
MEASURED CODING GAIN FOR SUBOPTIMAL ENTROPY CODER.

Sequence	Measured PSNR Gain in dB		
	More Optimal	Suboptimal	Less Optimal
BasketballDrill	0.097	0.097	0.318*
BQMall	0.246	0.248	0.280
FourPeople	0.297	0.299	0.345
Kristen&Sara	0.391	0.395	0.455
PartyScene	0.172	0.172	0.175
Vidyó	0.379	0.384	0.612

\* This entry is obtained when quantizing step size is set to 500 rather than the default value of 1000 due to stability issues in implementation.

## IV. DISCUSSION

### A. Extension to Reshaping Functions with Multiple Pieces

This paper has investigated the class of reshaping functions that have only one piece of a linear segment with a nonzero

slope as shown in Fig. 2. In practice, reshaping functions with multiple pieces of linear segments are adopted in the VVC/H.266 standard. Our theoretical analysis of MSE and entropy is amendable to the multiple-segment scenario. However, as the number of segments increases, boundary analysis starts to become complicated, which lowers the mathematical tractability and may make the theoretical result less elegant. Nevertheless, it is possible to use simulated data to validate the phenomenon that we have derived and observed in the one-piece scenario. We leave both of these investigations to future work.

### B. Mild Quantization Effect in the Codomain of Reshapers

In the actual implementation of the reshapers in the VVC/H.266 standard, reshapers  $g$  and  $g^{-1}$  are implemented by lookup tables that generate integer-valued output. These integer-valued outputs exhibit a mild quantization effect. To



simplify our investigation, this paper skips such an effect. However, we note that the impact of the quantization should have a mild impact on the theoretical results.

### C. Choice of Evaluation Metrics

We choose the cosine similarity [31] as the evaluation metric to verify the proposed theoretical model via the experiments. The cosine similarity focuses on the consistency between the theoretically predicted gain and the experimentally measured gain. This is in line with this paper's goal of providing a theoretical justification for the performance enhancement achieved through the adoption of the in-loop reshapener. We did not use metrics that are sensitive to the specific magnitudes of gains or losses, including MSE, mean absolute error (MAE), and Pearson's correlation [31]; instead, we prioritize a metric that can consistently distinguish between gains and losses. Although being able to predict the precise magnitudes of gains is advantageous, it can be technically challenging to accomplish, considering the complex architecture of video codecs. Another drawback of using Pearson's correlation as the evaluation metric is that its score discards the average signal level when calculating the similarity of two signals being compared [31, Ch. 2.4.5]. In contrast, cosine similarity measures the similarity by considering the context given by the average signal level, which is the achieved PSNR gains' average that our study focuses on.

We also note that other metrics such as Spearman's correlation and Kendall's correlation [32, Ch. 2] are unsuitable for the objectives of our work. Spearman measures the strength and direction of association between two ranked variables, but the exact rank of a predicted gain is not the key to verifying our theoretical result. Kendall's correlation is also a rank-based metric so it is less relevant.

## V. CONCLUSION

In this paper, we have theoretically analyzed the rate-distortion performance of the in-loop reshapener and have proved that coding efficiency can be improved only when the entropy coder is suboptimal—the scenario that video coding practically deals with. We have derived the PSNR gain in the closed form and have shown that the theoretically predicted gain is consistent with that measured from experiments using standard testing video sequences.

## REFERENCES

- [1] *Recommendation H.266, Versatile Video Coding (VVC)*, ITU-T/ISO/IEC Std., 2020.
- [2] *Recommendation H.265, High Efficiency Video Coding (HEVC)*, ITU-T/ISO/IEC Std., 2013.
- [3] X. Xiu, P. Hanhart, R. Vanam, Y. He, Y. Ye, T. Lu, F. Pu, P. Yin, W. Husak, and T. Chen, "Description of SDR, HDR, and 360° video coding technology proposal by InterDigital Communications and Dolby Laboratories," ISO/IEC JTC1/SC29/WG11 MPEG, San Diego, USA, Tech. Rep. J0015, Apr. 2018.
- [4] T. Lu, F. Pu, P. Yin, W. Husak, S. McCarthy, and T. Chen, "CE12: HDR in-loop reshaping," ISO/IEC JTC1/SC29/WG11 MPEG, Ljubljana, Slovenia, Tech. Rep. K0308, Jul. 2018.
- [5] T. Lu, F. Pu, P. Yin, W. Husak, and S. McCarthy, "SDR in-loop reshaping," ISO/IEC JTC1/SC29/WG11 MPEG, Ljubljana, Slovenia, Tech. Rep. K0309, Jul. 2018.
- [6] T. Lu, F. Pu, P. Yin, T. Chen, and W. Husak, "Adaptive reshaping for next generation video codec," in *SPIE Applications of Digital Image Processing XLI*, vol. 10752, San Diego, CA, Sep. 2018.
- [7] F. Dufaux, P. Le Callet, R. Mantiuk, and M. Mrak, *High Dynamic Range Video: From Acquisition, to Display and Applications*. Academic Press, 2016.
- [8] *Recommendation H.264, Advanced Video Coding (AVC)*, ITU-T/ISO/IEC Std., 2003.
- [9] A. Luthra, E. François, and W. Husak, "Draft call for evidence (CfE) for HDR and WCG video coding," ISO/IEC JTC1/SC29/WG11 MPEG, Geneva, Switzerland, Tech. Rep. N15083, Feb. 2015.
- [10] D. Baylon, Z. Gu, A. Luthra, K. Minoo, P. Yin, F. Pu, T. Lu, T. Chen, W. Husak, Y. He *et al.*, "Response to call for evidence for HDR and WCG video coding: Arris, Dolby and InterDigital," ISO/IEC JTC1/SC29/WG11 MPEG, Warsaw, Poland, Tech. Rep. M36264, Jun. 2015.
- [11] —, "CE2.1.1: Single layer HDR-only solution based on m36264," ISO/IEC JTC1/SC29/WG11 MPEG, Geneva, Switzerland, Tech. Rep. M37070, Oct. 2015.
- [12] D. Rusanovskyy, S. Lee, D. Bugdayci, A. Ramsabramonian, J. Sole, M. Karczewicz, A. Tourapis, Y. Su, D. Singer, C. Fogg *et al.*, "Single layer non-normative (category 3a) NCL and CL responses to the call for evidence on HDR/WCG," ISO/IEC JTC1/SC29/WG11 MPEG, Warsaw, Poland, Tech. Rep. M36256, Jun. 2015.
- [13] A. Ramasubramonian, J. Sole, M. Karczewicz, S. Lee, D. Rusanovskyy, D. Bugdayci, and X. Li, "Dual layer non-normative (category 3b) response to the call for evidence on HDR/WCG," ISO/IEC JTC1/SC29/WG11 MPEG, Warsaw, Poland, Tech. Rep. M36280, Jun. 2015.
- [14] S. Lasserre, F. Le Leannec, E. Francois, and T. Poirier, "Technicolor's response to CfE for HDR and WCG (category 1)," ISO/IEC JTC1/SC29/WG11 MPEG, Warsaw, Poland, Tech. Rep. M36263, Jun. 2015.
- [15] R. Goris, R. Brondijk, and R. van der Vleuten, "Philips response to CfE for HDR and WCG," ISO/IEC JTC1/SC29/WG11 MPEG, Warsaw, Poland, Tech. Rep. M36266, Jun. 2015.
- [16] A. Cotton, T. Borer, M. Pindoria, S. Thompson, M. Naccari, S. Schwarz, and M. Mark, "BBC's response to CfE for HDR video coding (category 3a)," ISO/IEC JTC1/SC29/WG11 MPEG, Warsaw, Poland, Tech. Rep. M36249, Jun. 2015.
- [17] J. Strom, J. Samuelsson, M. Pettersson, K. Andersson, P. Wennersten, and R. Sjoberg, "Ericsson's response to CfE for HDR and WCG," ISO/IEC JTC1/SC29/WG11 MPEG, Warsaw, Poland, Tech. Rep. M36184, Jun. 2015.
- [18] T. Lu, F. Pu, P. Yin, W. Husak, S. McCarthy, and T. Chen, "CE12-2: Hdr in-loop reshaping," ISO/IEC JTC1/SC29/WG11 MPEG, Macao, China, Tech. Rep. L0245, Oct. 2018.
- [19] T. Lu, F. Pu, P. Yin, W. Husak, and S. McCarthy, "CE12-4: Sdr in-loop reshaping," ISO/IEC JTC1/SC29/WG11 MPEG, Macao, China, Tech. Rep. L0246, Oct. 2018.
- [20] —, "CE12: Mapping functions (test CE12-1 and CE12-2)," ISO/IEC JTC1/SC29/WG11 MPEG, Marrakech, Morocco, Tech. Rep. M0427, Jan. 2019.
- [21] T. Lu, F. Pu, P. Yin, W. Husak, S. McCarthy, and T. Chen, "Simplification of reshapener implementation," ISO/IEC JTC1/SC29/WG11 MPEG, Geneva, CH, Tech. Rep. N0220, Mar. 2019.
- [22] T. Lu, F. Pu, P. Yin, S. McCarthy, W. Husak, T. Chen, E. Francois, C. Chevance, F. Hiron, J. Chen, R. Liao, Y. Ye, and J. Luo, "Luma mapping with chroma scaling in versatile video coding," in *Data Compression Conference (DCC)*, 2020, pp. 193–202.
- [23] B. Bross, J. Chen, S. Liu, and Y.-K. Wang, "Versatile video coding (draft 10)," ISO/IEC JTC1/SC29/WG11 MPEG, Teleconference, Tech. Rep. S2001, Jul. 2020.
- [24] R. C. Gonzales and R. E. Woods, *Digital Image Processing*. Pearson, 2008.
- [25] B. Bross, Y.-K. Wang, Y. Ye, S. Liu, J. Chen, G. J. Sullivan, and J.-R. Ohm, "Overview of the Versatile Video Coding (VVC) standard and its applications," *IEEE Transactions on Circuits and Systems for Video Technology*, vol. 31, no. 10, pp. 3736–3764, 2021.
- [26] C.-W. Wong, G.-M. Su, and M. Wu, "Impact analysis of baseband quantizer on coding efficiency for HDR video," *IEEE Signal Processing Letters*, vol. 23, no. 10, pp. 1354–1358, Oct. 2016.
- [27] A. K. Jain, *Fundamentals of Digital Image Processing*. Prentice-Hall, Inc., 1989.
- [28] B. Widrow and I. Kollár, *Quantization Noise: Roundoff Error in Digital Computation, Signal Processing, Control, and Communications*. Cambridge University Press, 2008.

- [29] T. M. Cover and J. A. Thomas, *Elements of Information Theory*. Wiley-Interscience, 2006.
- [30] G. Grimmett and D. Stirzaker, *Probability and Random Processes*. Oxford university press, 2020.
- [31] P.-N. Tan, M. Steinbach, and V. Kumar, *Introduction to Data Mining*. Pearson Addison Wesley, 2006.
- [32] M. G. Kendall and J. D. Gibbons, *Rank Correlation Methods*. Oxford university press, 1990.